frontiers | Frontiers in Materials

TYPE Original Research
PUBLISHED 08 February 2023
DOI 10.3389/fmats.2023.1057637

OPEN ACCESS

EDITED BY
Dong Zhang,
Fuzhou University, China

REVIEWED BY
Mehmet Serkan KIRGIZ,
Istanbul Sabahattin Zaim University, Türkiye
Ali Shokrgozar,
Idaho State University, United States

*CORRESPONDENCE
Muhammad Abid,
abidkhg@gmail.com

SPECIALTY SECTION
This article was submitted to Structural Materials, a section of the journal Frontiers in Materials

RECEIVED 29 September 2022
ACCEPTED 19 January 2023
PUBLISHED 08 February 2023

CITATION
Khan MNA, Malik AH, Yaqub M, Umar M, Noman M, Abid M, Alabduljabbar H, Mohamed A and Zaidi SSA (2023), Development of high-temperature heavy density dolerite concrete for 4th generation nuclear power plants. *Front. Mater.* 10:1057637. doi: 10.3389/fmats.2023.1057637

Development of high-temperature heavy density dolerite concrete for 4th generation nuclear power plants

Muhammad Nasir Ayaz Khan[1], Azhar Hussain Malik[2], Muhammad Yaqub[1], Muhammad Umar[4], Muhammad Noman[3], Muhammad Abid[5]*, Hisham Alabduljabbar[6], Abdullah Mohamed[7] and Syed Salman Ahmad Zaidi[8]

[1]Civil Engineering Department, University of Engineering and Technology, Rawalpindi, Pakistan, [2]Department of Nuclear Engineering, Pakistan Institute of Engineering and Applied Sciences, Islamabad, Nilore, Pakistan, [3]Department of Civil Engineering, Faculty of Engineering and Technology, International Islamic University Islamabad, Islamabad, Pakistan, [4]Civil Engineering Department, Zhengzhou University in Zhengzhou, Harbin, China, [5]College of Aerospace and Civil Engineering, Harbin Engineering University, Harbin, China, [6]Department of Civil Engineering, College of Engineering in Al-Kharj, Prince Sattam bin Abdulaziz University, Al-Kharj, Saudi Arabia, [7]Research Centre, Future University in Egypt, New Cairo, Egypt, [8]Civil Engineering Department, Wah Engineering College, University of Wah, Wah Cantonment, Pakistan

This study examines the physical, mechanical, microstructural, and attenuation properties of high-density concrete exposed to temperatures ranging from 200°C to 1200°C. For this purpose, heavy-density concrete containing 25%, 50%, 75%, and 100% dolerite aggregates was developed and compared with three ordinary concrete mixes. Pre- and post-heated concrete specimens were evaluated for mass and density loss, compressive strength, rebound hammer, X-ray and gamma-ray attenuation, Half Value Layer (HVL), and Ten Value Layer (TVL) along with microstructural properties determined by scanning electron microscopy and Energy Dispersive X-ray. The results showed that the incorporation of 75% dolerite aggregate during pre- and post-heating yielded high compressive strength whereas low mass and density loss. The same mixture showed significant improvement in gamma ray shielding at all temperatures. The Half Value Layer and Ten Value Layer values showed a reduction in the thickness of concrete as a shield. It is recommended that dolerite heavy-density concrete is a potential radiation shield at high temperatures ranging from 200°C–1200°C in fourth-generation nuclear power plants.

KEYWORDS

compressive strength, heavy-density concrete, x-ray, gamma ray, nuclear power plants, half value layer (HVL), temperature, attenuation

1 Introduction

Due to the increasing application of gamma rays in studying the biologically harmful effects, several studies have already been performed on the shielding properties of various materials (Mollah et al., 1992; Gökçe et al., 2018; Moharram et al., 2020). Among all materials, concrete is widely accepted as a shield against gamma radiation due to its high strength, acceptable density, and inexpensive design flexibility (Tekin et al., 2018). However, the properties of concrete as a radiation shield, for instance, density, depend upon the composition of materials in concrete. Therefore, in the recent past, many studies have been devoted to developing concrete shields by

TABLE 1 Physical and chemical properties of cement.

Chemical composition	Values (%)	Physical properties	Value
CaO	57.35	Specific gravity (g Cm−3)	3.12
SiO2	20.30	Average particle size (μm)	18
Al2O3	9.24	Blaine fineness (Cm2 g-1)	3152
MgO	3.02	Initial setting time	1 h and 25 min
Fe2O3	3.61	Final setting time	3 h and 48 min
SO3	2.98	Consistency (%)	31
Na2O	0.25		

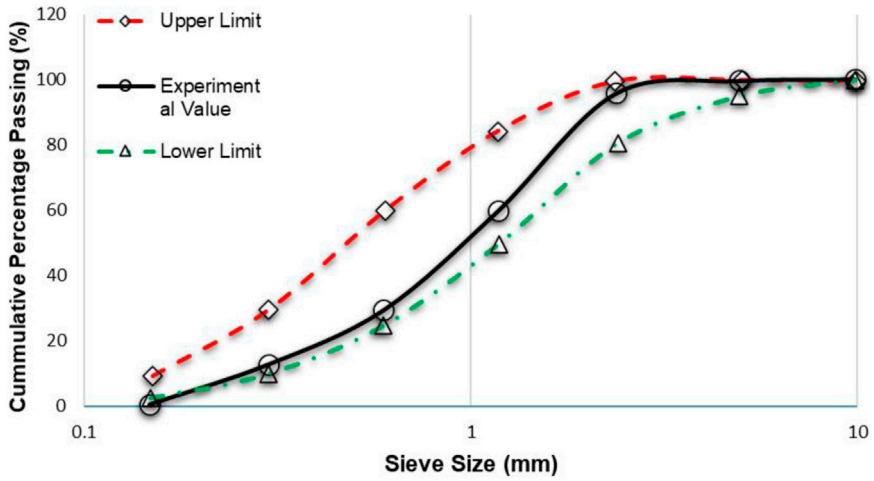

FIGURE 1
Gradation curves of fine aggregate.

introducing various types of special aggregates i e., natural such as magnetite (Thomas et al., 2019), barite (Almeida et al., 2017), serpentine (Kansouh 2012) as well synthetic aggregate like steel shots (Maslehuddin et al., 2013), steel furnace slag (Khalaf et al., 2019) Heavyweight concrete has a density greater than 2600 kg/m^3 (Lotfi-omran et al., 2019). The recent developments in heavyweight concrete have been explained in detail by (Malik et al., 2022).

Heavyweight aggregates are used to fabricate heavy-density concrete for the construction of radiation shielding (Horszczaruk, 2019). developed magnetite concrete as a radiation shield showed 11.7% higher attenuation of gamma rays than barite concrete and 44.8% than ordinary concrete (El-Samrah et al., 2018). fabricated barite-limonite concrete and concluded that the linear attenuation coefficient rises with increasing temperature up to 450°C. A prior study on barite concrete suggested that approximately 40% of wall thickness could be decreased compared to walls fabricated with ordinary concrete (Akkurt and El-Khayatt 2013). However, iron ores are expensive and difficult to work with (Gencel et al., 2012). Before utilization, these ores pass through many complex processes compared to traditional aggregates, such as mining, transportation from mines, screening, and cleaning. The other main problem is the diversity of aggregates in properties due to excavation location. Barite, for instance, may contain 90% $BaSO_4$ as well as 65% $BaSO_4$. Thus, concretes fabricated due to different properties in aggregates behave differently (Sikora et al., 2019). For these reasons, there is a clear need to develop heavy-density concrete utilizing other materials, preferably waste materials that are less expensive and serve as decent radiation shields with good mechanical properties (Gencel et al., 2012).

On the one hand, careful selection should be made while fabricating heavyweight concrete, as fabrication is a more critical process than conventional concrete. Each constituent, such as water, cement, and coarse aggregate, must be evaluated, whereas type and amount are the key consideration in the mixes (Khalaf et al., 2021). Water cement ratio is an important parameter in high-strength and high-density concrete preparation. However, the literature on improving concrete density by decreasing the water-cement ratio is scarce. Nevertheless, the water-cement ratios in heavyweight concrete range between 35% and 50% (Facure and Silva, 2007). A study concluded that the optimum water-cement ratio for barite concrete is 0.40 (Topçu, 2003). At the same time, the quality and type of cement also matter in the fabrication of heavyweight concrete because the cement content in heavyweight concrete is that it must be high enough to prevent any radiation seepage while low enough to affect shrinkage. For such reasons, 350 kg/m^3 is the recommended cement content for heavyweight concrete (Celik et al., 2015). However, barite and magnetite

TABLE 2 Physical and chemical properties of DHA.

Chemical analysis	Values (%)	Physical properties	Value
SiO2	46.12	Specific gravity (g Cm−3)	3.05
Al2O3	16.21	Bulk density (g Cm−3)	3.96
Fe2O3	16.45	Hardness (Moh's Scale)	9
CaO	7.8	Melting point °C	1430
MgO	5.3	Color	Grey
Na2O	3.4	Shape	Angular
Others	3.70	Water absorption (smooth)	0.9%
Total	98.98	Water absorption (porous)	2.3%

concrete required high cement content between 400 and 490 kg/m^3 to reach the desired strength (Ouda 2015; Yao et al., 2016). Moreover, heavyweight concrete can be developed using any Portland cement; however, cement produced from coarsely ground clinker should be avoided (Horszczaruk, 2019). Concretes fabricated with a cement content of 350–400 kg/m^3, the typical values of densities for some concretes are.

- steel scrap - 6–6.500 g/cm^3 (fc = 75 MPa, w/c = 0.29) (González-Ortega et al., 2014)
- barite + steel scrap—4.50–5.0 g/cm^3 (fc = 35–50 MPa, w/c = 0.3–0.4) (Kilincarslan et al., 2006)
- iron ore—4.0 g/cm^3 (fc = 75–80 MPa, w/c = 0.40) (Shirayama, 1963)
- magnetite - >3.50 g/cm^3 (fc = 75–80 MPa, w/c = 0.30) (Ouda 2015)
- limonite + steel shot - >3.50 g/cm^3 (fc = 60 MPa, w/c = 0.40) (lo Monte et al., 2014)
- barite or magnetite—3.50 g/cm^3 (fc = 35–45 MPa, w/c = 0.37–0.60) (lo Monte et al., 2014)
- copper slag aggregate—2.80–3.0 g/cm^3 (fc = 70–95 MPa, w/c = 0.33–0.45) (Behnood 2014)

Nuclear power plants (NPPs) are subjected to high temperatures during their entire operating life. High temperatures induce complex changes such as mass and strength loss in concrete due to loss of bound and unbound water from the hydrated products of cement. Exposure to high temperatures, calcination of calcareous aggregates, and volumetric instability of quartz aggregates are necessary changes that trigger mass and strength loss phenomena (Fillmore 2004). The more the loss in mass and strength, the more the density reduction, ultimately reducing the radiation shield's attenuation capability (Nikbin, 2020). Most NPPs operate at a temperature of 65°C; this situation could be worsened in case of any emergency or fire. The thermal properties of concrete get importance in the case of high-temperature reactors where temperature can reach 400°C in thick pre-stressed concrete shields in nuclear reactors (Sakr and El-Hakim 2005). Whereas the thermal properties of ordinary concrete have been the subject of investigation in the past, their parameters are well known. Increasing temperatures more than 100°C, the vapor pressure developed due to water inside the concrete increasing internal pressure, leading to cracking in concrete and sometimes spalling at high temperatures. Increasing temperature above 300°C leads to some severe changes inbound and unbound water to concrete. In contrast, considerable deterioration and degradation in strength have been reported in concrete exposed to a temperature above 600°C. The elastic modulus and compressive strength drop to half by increasing temperature beyond 700°C (Mehdipour et al., 2020). Likewise, in recent times, exposure of heavyweight concrete to high temperatures has been a subject of interest for many. For instance (Thomas et al., 2019), developed magnetite concrete and subjected it to high temperatures to measure its physical and mechanical properties. Up to 300°C, the temperature had no influence on concrete's physical and mechanical qualities, but at 500°C, 80% of its initial compressive strength was lost. The breakdown of portlandite $(CaOH)_2$ into carbon dioxide (CO_2) and calcium oxide caused a considerable loss of strength and structural deterioration between 500°C and 700°C (CaO). At 800°C, C-S-H gel decomposes while maintaining 50% of its initial strength. A recent study (Horszczaruk and Brzozowski 2019) found that magnetite concrete maintained its phase stability up to 570°C without losing strength. Magnetite concrete loses 20% of its strength at 800°C (Kodur and Agrawal 2016). There is still a knowledge gap in heavyweight concretes exposed to temperatures above 800°C (Demir, Gümüş, and Gökçe 2020; lo Monte et al., 2014).

Artificial aggregates, such as steel shots and iron pellets, do, in fact, increase the density of concrete more than natural aggregates. However, there are certain limitations to using artificial aggregates, such as the compaction of fresh concrete due to gap-graded aggregates, and iron and steel must be rusted before use in order to form strong bonds with other concrete ingredients (Lerman et al., 2020). Another factor is magnetic attraction, which interferes with the interlocking effect of steel or iron with other particles (Rohrig, 2016). As a result, natural aggregates can be utilized as heavy-density aggregates in concrete as gamma ray shields.

Based on the authors' knowledge, it can be concluded that waste or by-product aggregates with sufficient density could be used in gamma radiation shields to overcome the limitations explained in the literature. Utilization of waste and by-products is sustainable, environmentally friendly, and cost-effective approach. For this reason, Dolerite Heavyweight Aggregates (DHA) with a density of 3.12 g/cm^3 is utilized in concrete. The concrete is subjected to high temperatures from 200°C to 1200°C. The physio-mechanical properties (compressive strength, rebound hammer, mass, and density loss), as well as their ability to absorb harmful radiation (linear and mass attenuation coefficients, Half Value Layer (HVL), and 10th Value Layer (TVL)) for pre- and post-heated, concretes were analysed. Apart from that, to evaluate the chemical changes at a micro level, Scanning Electron Microscope (SEM) and X-ray

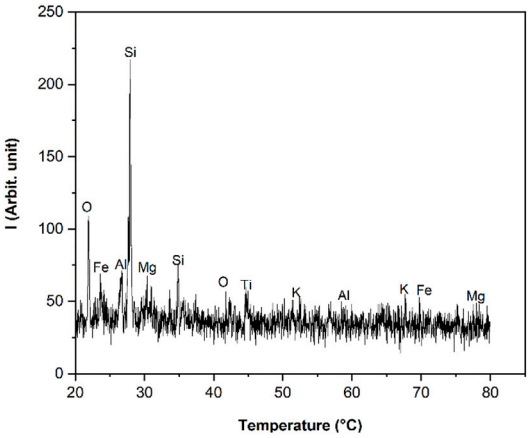

FIGURE 2
XRD analysis of DHA.

radiography for studying voids and cracks due to thermal changes are also part of this study. The evaluation of concrete shields at such high temperatures will help fulfill the current demand for the knowledge of fourth-generation nuclear power plants where temperatures can reach more than 1000°C (Thomas et al., 2019).

2 Materials and testing methodology

2.1 Materials

Ordinary Portland cement (OPC) ASTM Type 1, fouji brand, Pakistan, was used in the present study. The physical and chemical properties of the cement are given in Table 1, which shows the specific gravity value of 3.12 gm/cm^3.

Normal-weight limestone aggregate obtained from Margalla hills and fine aggregates from Lawarancepur, Pakistan were used in this research. The gradation curve of fine aggregates is shown in Figure 1. The gradation of fine aggregates is within the upper and lower limits defined by ASTM C33. Also, the fineness modulus calculated for fine aggregates is 2.7 which is also within limits.

To avoid harsh mixes and to achieve satisfactory consistency, Chemrite-SP 303 superplastisizer, Emporient Chemicals, was used.

Dolerite heavyweight aggregates (DHA) were obtained from two sources; one from the parent source (place of mining, located in Mansehra, KPK, Pakistan, situated (34° 25' 27″N, 72° 58' 05″E), while the other from a factory where these stones are cut and polished. So, there were two types of aggregates; one with a polished surface and the other with a coarse and rough surface. Trial mixes were prepared using both types of aggregates; however, concrete mixes prepared with polished surface aggregate tend to settle down in fresh mix due to no or very little inter-particles friction, resulting in mixes with no adhesion. Therefore, based on trials, a mixture of both types of aggregates was used to cast concrete. The density and other physical characteristics of DHA are shown in Table 2.

To study the phase identification of the crystalline nature of DHA, X-Ray diffraction (XRD) analysis was carried out in Centralized Resourced Laboratory (CRL), UoP, Pakistan, through JDX-3535 JOEL diffractometer. The peak positions of crystalline at 2-Alpha are plotted against the X-Ray counts (intensity) as shown in Figure 2. The figure shows that dolerite aggregates are rich in silica (Si) and Oxygen (O) contents. There are small traces of Magnesium (Mg), Aluminum (Al), Titanium (Ti), and Phosphorous (K). The element that contributes to the high density of dolerite aggregate is Iron (Fe) which could be found in abundance with various peaks.

2.2 Mixing details

In this study, seven mixes were considered to understand better the effect of high temperature on the mechanical properties of heavyweight concrete made with dolerite aggregates. The ratio of aggregates varied among the mixes. For instance, DC1 concrete indicates "dolerite concrete mix with 25% dolerite aggregate and 75% limestone aggregates. The other mixes designation is; DC2 (50% dolerite and 50% limestone), DC3 (75% dolerite and 25% limestone aggregate), and DC4 (100% replacement of limestone aggregates with dolerite aggregates). Control mix CM1 (5–9 mm limestone), CM2 (5–16 mm limestone), and CM3 (5–25 mm limestone) were also part of this study for comparison purposes.

The water-cement ratio w/c = 0.45 was kept constant for all mixes. The cement quantity (less than 400 kg/m^3) was the same for all the mixes. Chemrite SP-303 superplasticizer was introduced to get the acceptable consistency used for specimen preparation as per supplier recommendation (0.4%–1.5% by weight of cement). The mix design adopted in this study is shown in Table 3.

2.3 Specimen preparation

In this study, a total of 210 specimens were prepared for compressive testing for pre and post-heating in a furnace. The cylindrical specimens cast were 150 mm in diameter and 300 mm in length. Three specimens were poured for each mix and temperature, and the average value was taken at the end of each mix testing. Three specimens in each mix were exposed to 200°C, 400°C, 600°C, 800°C, 1000°C, and 1200°C.

For gamma-ray and X-ray attenuation, cubic specimens with dimensions 150 mm × 150 mm x 150 mm were poured. These specimens were then cut mechanically for 20 ± 2 mm thickness. This way, three specimens per mix per temperature with dimensions (150 mm × 150 mm x 20 ± 2 mm) were prepared. So, a total of 105 specimens were prepared for both gamma and X-ray attenuation. Specimens of each mix were exposed to 200°C, 400°C, 600°C, 800°C, 1000°C, and 1200°C temperatures. It may be noted that the same specimens were tested first for X-ray and then gamma rays attenuation. Before testing, all the specimens (315 No's) for mechanical and attenuation properties were cured in a water tank under controlled laboratory conditions.

2.4 Heating procedure for concrete specimens

The heating process was carried out in a trolley-operated electric furnace having dimensions of 500 mm × 600 mm × 1200 mm. Before heating, the specimens were oven-dried at 110°C for 24 h to remove any free water. This is to prevent the concrete specimens from

TABLE 3 Mix design of control and DC mixes.

Concrete type	Aggregate ratio	W/c	Water (kg/m3)	Cement (kg/m3)	Fine aggregate (kg/m3)	Coarse aggregate (kg/m3)	DHA (kg/m3)	Superplasticizer (kg/m3)	Total (g/cm3)
CM1	100% limestone aggregates (5–9 mm)	0.4	153	388	712	1273	-	0.65	2.53
CM2	100% limestone aggregates (5–16 mm)	0.4	153	388	712	1288	-	0.65	2.54
CM3	100% limestone aggregates (5–25 mm)	0.4	153	388	712	1310	-	0.75	2.56
DC1	25% DHA +75% limestone (5–25 mm)	0.4	153	369	765	1014	388	0.76	2.69
DC2	50% DHA +50% limestone (5–25 mm)	0.4	153	361	752	714	776	0.88	2.76
DC3	75% DHA +25% limestone (5–25 mm)	0.4	153	388	874	318	1164	0.91	2.90
DC4	100% DHA (5–25 mm)	0.4	153	388	875	-	1552	0.96	2.97

exploding during the heating process in the furnace. The furnace is installed with a ventilator to circulate air from the atmosphere into the furnace. The door and outside walls of the furnace were installed with water-cooling pipes that constantly circulate to keep the doors and outside walls cooled and exploded due to overheating. Before heating, specimens were assessed for mass and density at room temperature. This was done after heating specimens in an oven at 110°C for 24 h to obtain constant mass by eliminating any free water. The specimens were then loaded from the front on the machine-operated trolley, and the furnace doors were sealed. The specimens were heated to the desired temperature of 200°C, 400°C, 600°C, 800°C, 1000°C, and 1200°C with a 3°C–5°C/min loading temperature. Afterward, reaching the desired temperature, the furnace temperature was held constant for 120 min. After heating, the doors were shut to bring the temperature of the furnace to room temperature, and the specimens were then unloaded. The concrete mixes were measured again for mass and density loss after they were cooled to room temperature. The specimens were measured for weight loss and visual observation after removal from the furnace. Compressive strength test (ASTM C39/C39M − 17b), rebound hammer (ASTM, C 805–02), and mass and density loss were conducted immediately.

2.5 X-ray radiography and gamma-ray attenuation coefficient

X-ray computed radiography of concrete to measure the three-dimensional dispersal of pores, air voids, and air pockets in solid materials is a non-destructive technique that has proven to be effective in pore characterization of porous materials. For the same reason, this study presents the x-ray imaging of heavyweight concrete subjected to high temperatures. So, the concrete specimens with 150 mm × 150 mm × 20 mm of ambient and high temperatures have been shifted to Metallographic Testing Lab (MTL), Non-destructive Testing (NTD) in Heavy Mechanical Complex (HMC) Taxila, Pakistan. The specimens covered in D7 film were put on a lead table with minimum noise to get a better and more concise image. The exposure time of X-ray radiation for this setup was 1 min. The scheme of the experimental setup is shown in Figure 3.

Concrete specimens' gamma rays' characteristics were tested in the Nuclear Engineering and Radiation Measurement Laboratory (NERML), Pakistan Institute of Engineering and Applied Sciences (PIEAS), Islamabad, Pakistan. The schematic procedure of gamma irradiation through a ^{137}Cs source with 0.622 MeV energy enclosed in the lead shield is shown in Figure 4. To avoid stray radiation from reaching the detector and making good geometry, two lead collimators were introduced in front of the source and the other in front of the detector. Both collimators were aligned using laser points. Before un-shielding the source, concrete specimens were placed vertically with 20 ± 2 mm thickness in front of the source. The un-collided gamma rays were detected by NaI (Ti) detector. The detector counted the emitted rays from the source passing through the collimators and penetrating through the specimen. The weak detector signals are required to be amplified by an amplifier (PMT) prior to shaping. Before that, aluminum and copper samples with known parameters were tested before actual concrete testing for the calibration of the experimental setup. For the accuracy of results, the selection of window channel on Single Channel Analyzer (SCA) played a valuable role. So, a pulse of height representing full energy peak is selected on SCA, which is counted by the counter-timer. A similar experimental setup has been published previously by (Ouda and Abdel-Gawwad, 2017; Khan et al., 2022).

The variations in the radiation intensity are measured through Lamber-Beer law given in Equation 1. To measure the gamma rays shielding effectiveness of concrete, the half-value layer (HVL) and

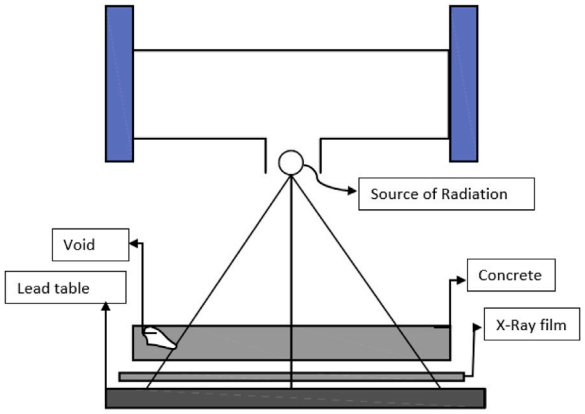

FIGURE 3
Schematic diagram of the X-ray test setup.

10th Value Layer (TVL) were measured through Eqs 2, 3 and respectively (Lamarsh et al., 2014; Singh and Singh, 2021)

$$I = I_0\, e^{-\mu x} \tag{1}$$

$$HVL = \frac{\ln(2)}{\mu} \tag{2}$$

$$TVL = \frac{\ln(10)}{2} \tag{3}$$

Given that

I = intensity of radiation, I_0 = intensity of radiation without thickness, x = Thickness of shield, μ = Linear attenuation coefficient of the specimen.

3 Result and discussion

3.1 Physical observations

The pre and post-heated concrete specimens were physically observed for color changes, cracks, aggregate expansion, and voids. DC3 Specimen exposed to temperatures from 600°C to 1200°C is shown in Figure 5.

It was observed that up to 400°C, no physical changes were noticed except for slight color variations. No surface cracks could be observed in this temperature range as only free water tends to evaporate.

However, exposing specimens to a temperature of 600°C, few hair lines cracks were observed for control mixes as well as dolerite concrete. This is because chemically bound water tends to evaporate, which triggers chemical reactions and, in turn, leads to physical changes such as cracks (Koťátková et al., 2016). The control mixes suffered more than dolerite mixes against thermal stresses. The breakage in the cement matrix and decomposition of C-S-H and $CaCO_3$ to CO_2 and CaO occurs at 800°C and above (Naus, 2010). These breakages and chemical changes alter the specimen color to a large extent. Also, the cracks were more visible and could be measured with ordinary measuring tools. However, the width of the cracks were pronounced for control mixes compared to dolerite concrete. Complete decomposition of concrete specimens was noticed for control mixes when exposed to moisture, and their strength could not be assessed. In contrast, dolerite concrete showed some strength which was 12% of its original strength. At 1200°C, both control and dolerite mixes were completely decomposed. A large amount of aggregate expansion, internal core degradation, and cracks were observed in mixes.

Figure 6 shows the D3 mix having 75% dolerite aggregates before and after heating to a temperature of 1200°C. The cross-section of the mix shows that dolerite aggregates have made a good bonding with the cement matrix. They are firmly attached and adhered to the rest of the concrete constituents. The magnified part of the specimen shows a dolerite aggregate well embedded in a cement matrix, which provided extra resistance against external loads at ambient temperature. The same mix, when heated at a temperature of 1200°C, showed a different scenario: a complete degradation of cement matrix with large and wide cracks. The delamination of dolerite aggregates from the cement matrix could also be observed in the magnified part. However, the dolerite aggregates could be seen unharmed during heating up to 1200°C because the melting temperature of dolerite is above 1200°C (Ingham, 2013).

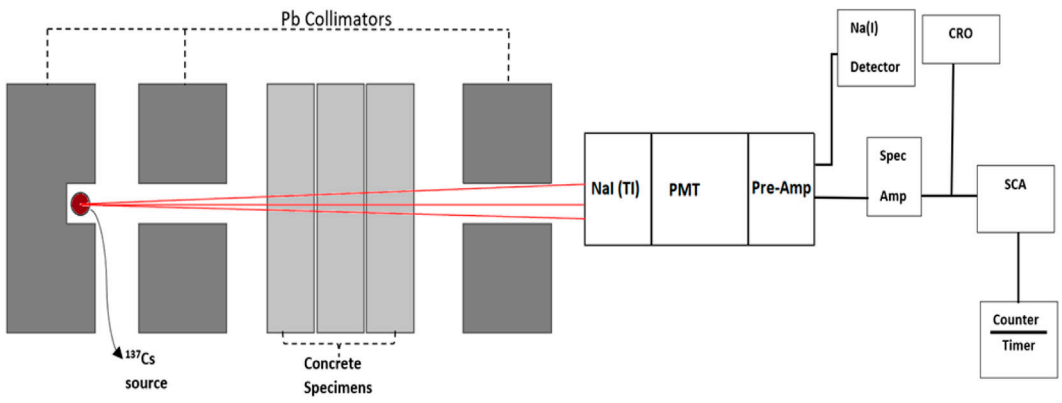

FIGURE 4
Systematic setup of gamma ray test.

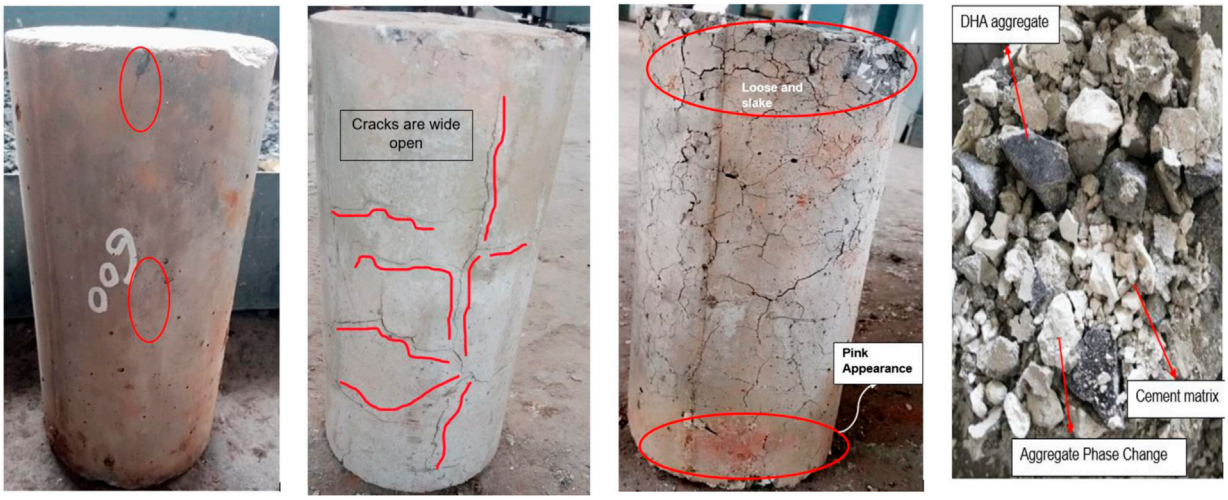

FIGURE 5
DC 3 mixes exposed to temperatures from 600°C to 1200°C.

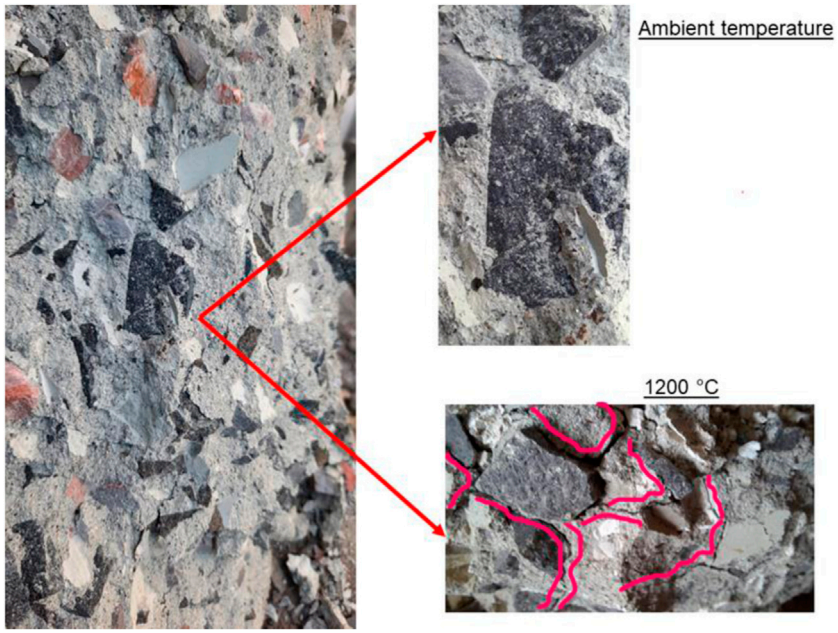

FIGURE 6
Delamination of DHA aggregates in Dolerite mix (D3) after exposed to 1200°C.

3.2 Mass and density loss

The mass and density loss of concretes were meaured before and after heating. The impacts of heating on mass and density loss of concrete were measured from 200°C to 1200°C is shown in Figures 7, 8, respectively. The mass and density loss followed a linear decrease with the variations in temperature. For instance, the density loss for CM1, CM2, and CM3 at 200°C showed a loss of −2%−1.5%, and−1.2%, respectively. No major loss in density has been observed at 400°C since only unbound or free water tends to evaporate from the mixes. Density loss has been increased to −12.4%−12.8% and−12.1% at 1000°C. Further heating of the specimens showed a major loss in density for CM1, CM2, and CM3 concrete, which was−16.6%−15.7%, and −14.9%. The high temperature has induced complex changes in concrete. The decomposition of C-S-H gel is one major reason for its loss of the chemically bound water, which decomposes the complex bonding of the cement matrix (Mohammed Haneefa et al., 2013).

On the other hand, due to the hard in nature and compact, dense structure of dolerite aggregates, the mixes sustain the elevated temperature as shown. For instance, compared to control mixes,

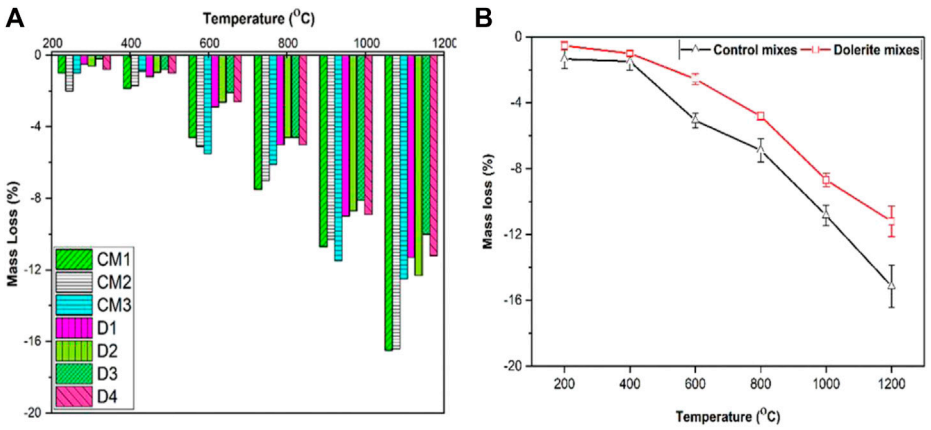

FIGURE 7
Mass loss of control and dolerite mixes as a function of temperature. **(A)** Mass loss **(B)** Mean and error as a function of temperature.

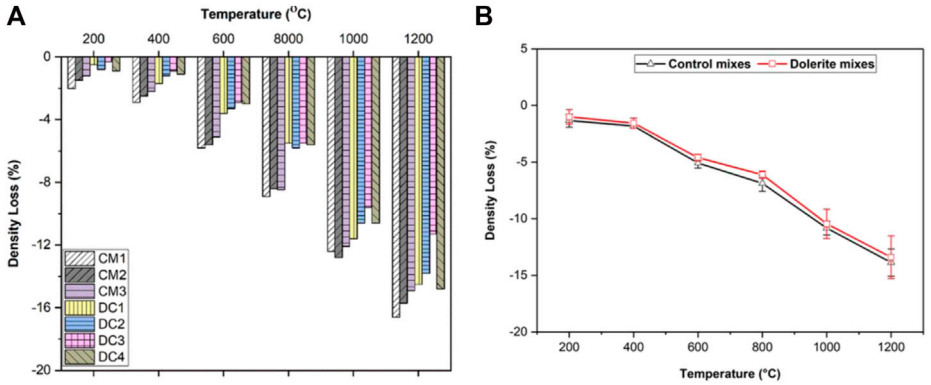

FIGURE 8
Density loss of control and dolerite mixes as function of temperature. **(A)** Density loss **(B)** mean and error bar as a function of temperature.

the D1, D2, D3, and D4 showed a density loss of −0.5%−0.8%−0.3%, and −0.9%, respectively. The density loss was not pronounced up to 600°C, maintaining its residual density up to 97%. Beyond 600°C, the D1, D2, D3 and D4 showed density losses of −11.6% −10.6% −9.6% and −10.6%, respectively. More severe changes have been observed at 1200°C, where the mixes retained 85.5%, 86.2%, 89.7%, and 86.8% of their initial density. It may be noted that the lowest density loss was observed for the D3 (having 75% dolerite aggregates) mix at low and high temperatures. The dolerite aggregates possess a rough and angular structure, providing extra resistance against thermal loads. Due to angular, they make a strong bond with the cement matrix and prevent the loss of hydrating water (Sloane, 1991).

3.3 Compressive strength

The compressive strength of control mixes and dolerite concrete as a function of temperature is shown in Figure 9 and mean values are depicted in Figure 10. At room temperature, dolerite concrete having 75% dolerite aggregates (D3) showed maximum strength among the specimens. The D3 mix showed a compressive strength of 57.6 MPa, more than the CM1, CM2, and CM3 mix by 31.9%, 29.3%, and 24.8%, respectively. The strength drops up to 400°C were not pronounced and showed a linear decrease in compressive strength. The strength values noted for D1, D2, D3, and D4 mixes were 40.94 MPa, 45.51 MPa, 52.704 MPa, and 48.42 MPa, respectively. Because, in this temperature range, the evaporation of free water, a rise in porosity, and dehydration of the C-S-H phase in the cement paste reduced the resistance (Shumuye et al., 2019) (Table 4).

Upon further heating, the mixes showed a rapid decrease in strength, which continued till 1200°C. The α-β-SiO_2- inversion occurs in the quartz crystals that make up the aggregate when the temperature reaches approximately 600°C. There is a 0.85%-point rise in the specific volume. The calcium hydroxide and other products of cement hydration start to dehydrate, which is one factor that contributes to the concrete structure's deterioration (Chang et al., 1994).

At 800°C, the strength loss for D1, D2, D3, and D4 concrete was found to be 53.0%, 50%, 55%, and 60% compared to ambient temperature strength. A 60% and 86% decrease was noted for D4 concrete at 800°C and 1000°C, respectively. As depicted in section 4.1, the delamination of dolerite aggregates occurs due to

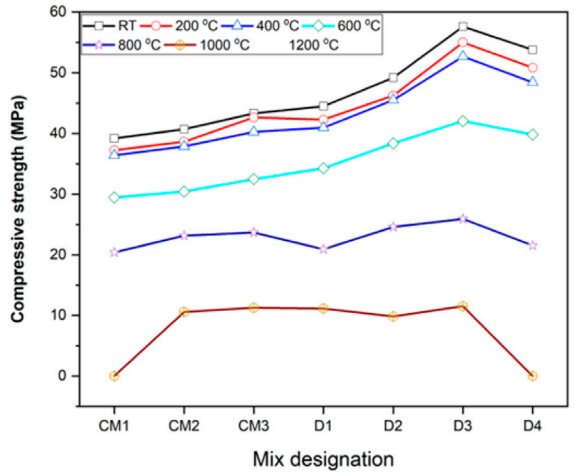

FIGURE 9
Compressive strength of control and dolerite mixes as function of temperature.

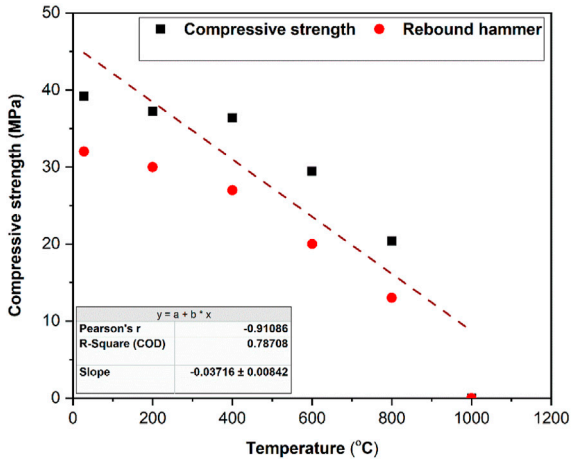

FIGURE 11
Correlation curve between compressive strength and rebound hammer for CM1 mix.

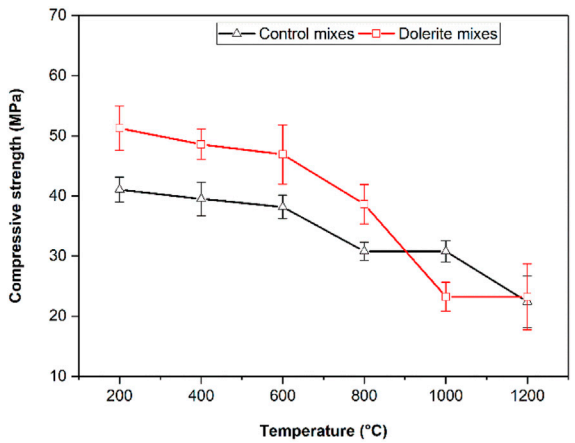

FIGURE 10
Mean and standard deviation of compressive strength against temperature.

extreme degradation in the cement core. Also, the calcium carbonate decomposes into CO_2, leading to further expansion of the specimen due to expansion in aggregates (Powe et al., 2020).

It may be shown that increasing the size of coarse aggregate tends to increase the compressive strength. For instance, CM1, CM2, and CM3 concrete showed a compressive strength of 39.2°MPa, 40.7°MPa, and 43.3 MPa at room temperature. The significant degradation in concrete was noted beyond the temperature at 400°C. Below 400°C, the residual strength of concrete specimens was found to be between 5%–7.1%. For instance, at 400°C, CM1, CM2, and CM3 concrete showed a loss in strength of 7.14%, 6.8%, and 6.9%, respectively of their initial values. However, at 600°C and beyond, the compressive strength decreased drastically, especially for CM1 mixes. At 600°C, 800°C, and 1000°C, the CM1 mixed showed a loss in compressive strength of 24.8%, 74.9%, and 100%, respectively. Where the highest compressive strength was noted for CM3 in this temperature range. At 600°C, 800°C, and 1000°C, a loss in compressive strength of 25%, 56%, and 73%, respectively, for CM3 mixes.

TABLE 4 Summary of test results with standard deviation.

Mix details	Compressive strength (MPa)		Mass loss (%)		Density loss (%)	
	Average	Standard deviation	Average	Standard deviation	Average	Standard deviation
CM1	46.90	4.23	−7.03	0.57	−8.10	0.59
CM2	44.70	3.11	−7.08	0.63	−7.75	0.77
CM3	43.16	5.94	−6.25	0.41	−7.33	1.27
DC1	35.26	4.87	−4.98	1.39	−6.23	1.61
DC2	22.88	2.03	−4.97	1.19	−5.92	1.16
DC3	10.29	1.36	−4.30	1.24	−5.08	1.67
DC4	2.79	2.68	−4.92	2.57	−6.00	1.15

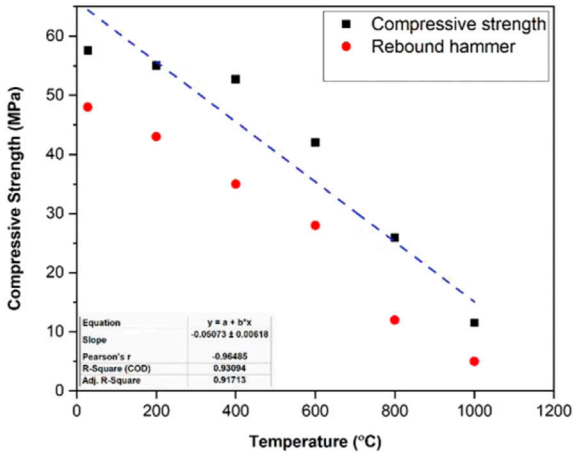

FIGURE 12
Correlation curve between compressive strength and rebound hammer for DC3 mix.

The strength could not be measured for the same mix at 1200°C due to complete decomposition of concrete. In addition, the gel has disintegrated, the structure of the cement paste has been damaged, as well as the structure is loose and slack in appearance (Hager 2013). At this temperature, the morphological behavior of the specimen is characterized by whitening of the specimen and appearance of fissures on the surface. At temperatures between 800°C and 1000°C, further disintegration and the formation of free and permeable material result in the creation of a significant number of long and wide fractures on the surface of the samples. With further exposure to moisture, the specimens are damaged and peeled off, a significant quantity of coarse aggregate is stripped off the cement paste, and the interfacial adhesion force is reduced or even gone (Burrow et al., 1979; Naus, 2010).

3.4 Rebound hammer

The results of rebound hammer in correlation with compressive strength for CM1 mix are shown in Figure 11. The rebound hammer for the CM1 mix was determined for temperatures between 28°C and 1000°C. The cumulative relation between compressive strength and rebound hammer yields an R-squared value of 0.787. The R-squared value is less than the DC3 mix, which is 0.93; this is because, beyond 600°C, a drastic decrease in compressive strength has been observed. The rebound values seem to follow the compressive trend. Increasing the temperature tends to decrease the rebound numbers. Up to 400°C, the values of the rebound hammer could be turned as a "good layer" beyond this temperature; all the values were termed as "fair," "poor," and "delaminated" at temperatures 600°C, 800°C, and 1000°C, respectively.

Figure 12 shows the variations of rebound hammer against temperatures for DC3 mix. Recalling the previous sections, this mix was qualified as the highest compressive strength mix with low mass and density loss. The rebound hammer and compressive strength R-squared were obtained as 0.930, which shows a good agreement between compressive and rebound values.

3.5 X-ray radiography

X-ray radiography is a conventional and highly effective non-destructive test (NDT) for measuring concrete defects such as air pockets, air voids, matrix, and bond cracks. Concrete underwent X-ray radiography to verify the qualities of the CM1 and DC3 mixes specified in sections 4.1, 4.3, and 4.4.

Figure 13A depicts a compact, dense construction with no gas pores and voids at a minimum. In the dark, the dolerite aggregates could be observed. No bonds or matrix cracks could be identified at this stage. Figure 13B displays a considerable number of cracks (shown in red), but no matrix cracks have yet emerged as a result of intense heating at 1000°C. The size of the gas pores (indicated in black) increases. At 1000°C, two types of cracks were seen in the CM1 mixture: matrix cracks and core cracks. The matrix cracks are marked in red. Due to intense heating, the border layer of concrete in the concrete disintegrated. In addition, many core fractures (marked in black) may be noticed in the concrete along with pores and voids (Hernandez-Murillo et al., 2020) as shown in Figure 13C.

3.6 Scanning electron microscopy (SEM)

The SEM analysis for the DC3 mix at ambient temperature is shown in Figure 14A. It could be shown that particles are induced into each other and make a strong bond against external resistance. It was discovered that the transition zone exhibited an entire matrix composed of ettringite, portlandite, and calcium silicate hydrate at ambient temperature. The white clouds are evidence of S-C-H gel formation in mixes. This concrete demonstrated the highest compressive strength at ambient temperature, which was 57.6 MPa. The EDX analysis was also taken of the same mix where traces of Fe, Si, Ca, Ti, and some minor traces of K and Al were found, as shown in Figure 15.

When the temperature reaches 1200°C, a significant proportion of water is evaporated, and many holes develop on the gelled layer in DC3 mix. In addition, the gel has disintegrated, the structure of the cement paste has been damaged, and the structure is loose and slack in appearance. In such temperatures, the macroscopic performance of the specimen exhibits whitening the specimen and the appearance of cracks on the surface of the specimen (Sivathanu Pillai et al., 2016), as shown in Figure 14D.

The CM1 mix at ambient temperature is shown in Figure 14B, where white clouds of C-S-H could be observed. Additionally, there are black holes identified in the mixes, which could be voids which depicts porous structure that results in low compressive strength compared to other mixes. The SEM analysis of the control mix (CM1) at 1200°C is shown in Figure 14C. At this stage, it is possible to identify the lack of cohesion and the friable, porous appearance of the C-S-H matrix and to identify some altered portions of the samples. As shown, there is no cohesion left between the particles, and complete degradation has been noticed.

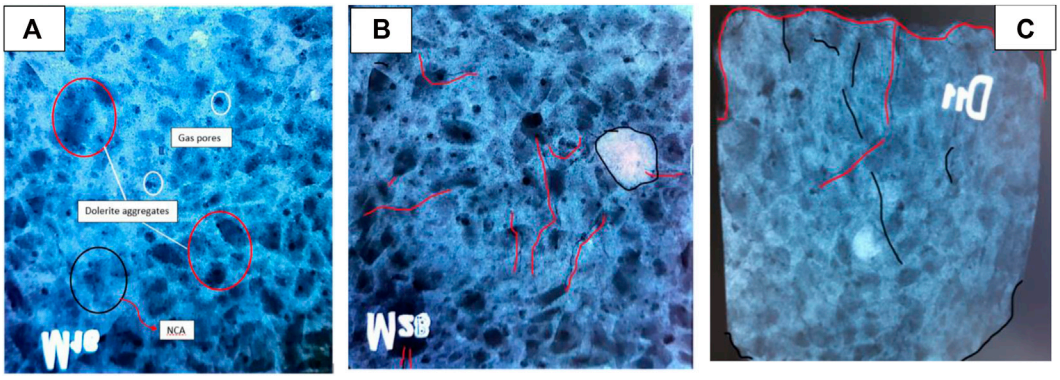

FIGURE 13
X-ray radiography **(A)** DC3 mix at ambient temperature, **(B)** Control mix at 1000°C and **(C)** DC3 mix at 1000°C.

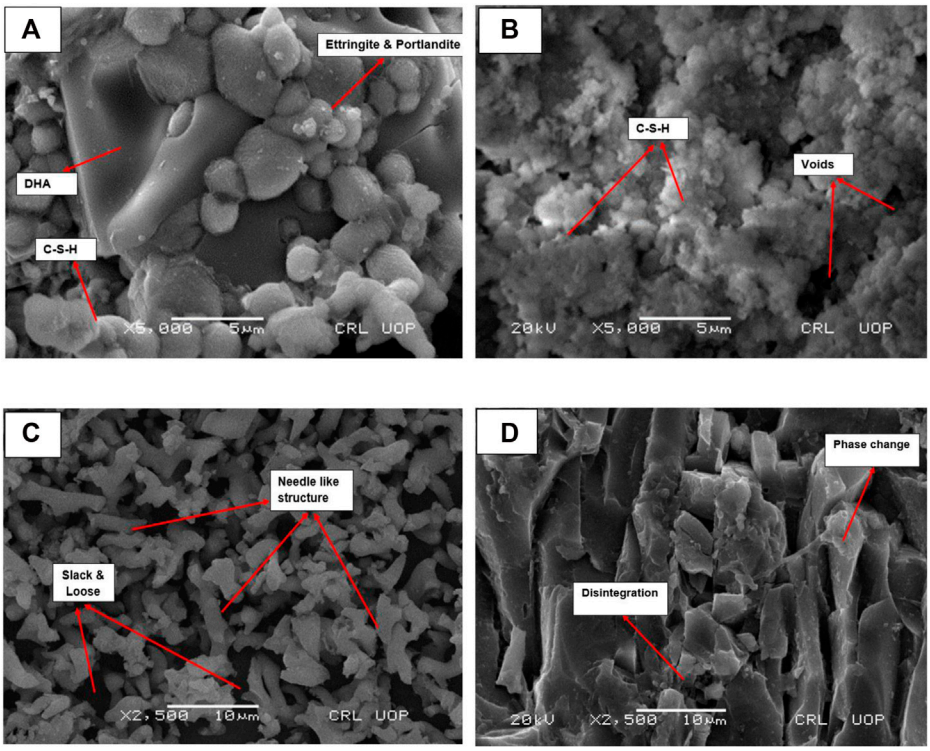

FIGURE 14
SEM analysis **(A)** DC3 mix at ambient temperature, **(B)** control mix at ambient temperature, **(C)** control mix at 1200°C, **(D)** DC3 mix at 1200°C.

High temperatures also affect the non-hydrated cement particles in the hydrated cement paste, causing them to expand more rapidly. Together with shrinkage in cement paste produced by variations in C-S-H and CH, this process promotes differential thermal expansion among the ingredients, resulting in microcracking and an increase in the porosity of the concrete mix (Diamond and Huang 2001). The cement mixture begins to melt at such high temperatures. Moreover, concrete specimens develop significant microstructure gaps and an interfacial transition zone between the aggregate and the cementitious matrix (Sadrmomtazi et al., 2012).

3.7 Gamma-ray attenuation

The gamma-ray attenuation was measured only for mixes that exhibited high and low compressive strength among all mixes at various temperatures. For this reason, DC3, DC4 and CM1concrete specimens were measured for gamma ray attenuation.

3.7.1 Linear attenuation coefficient (LAC)

The linear attenuation coefficient of CM1, DC3, and DC4 concrete is shown in Figure 16. The lowest linear

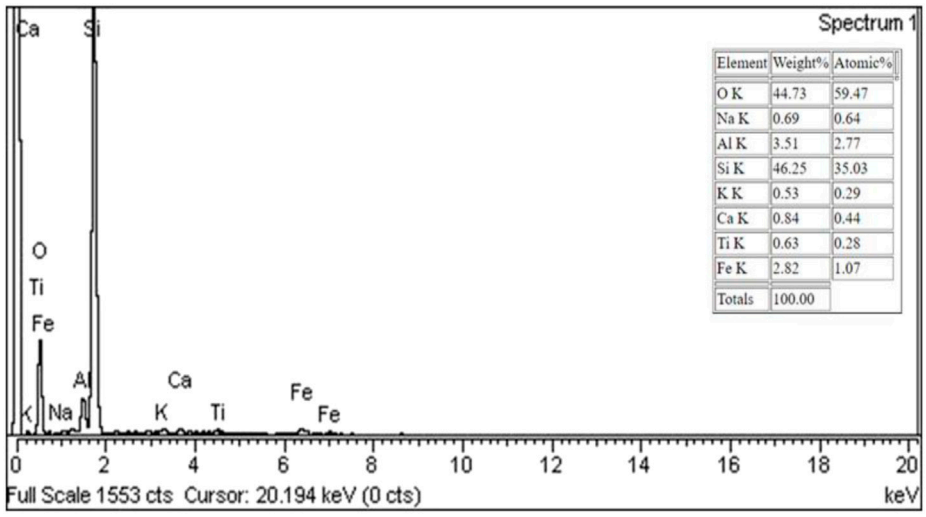

FIGURE 15
EDX analysis of DC3 mix at ambient temperature.

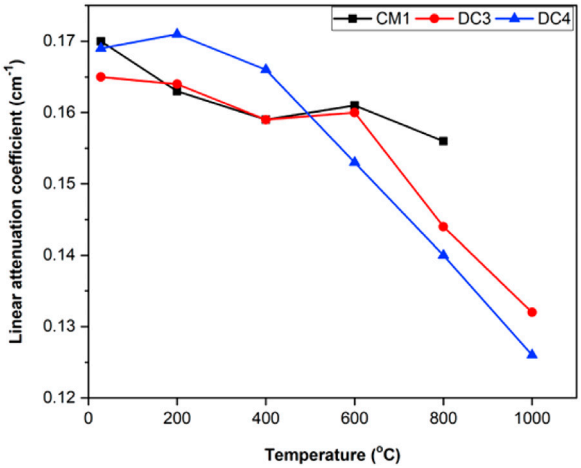

FIGURE 16
Linear Attenuation Coefficient (LAC) as function of temperature.

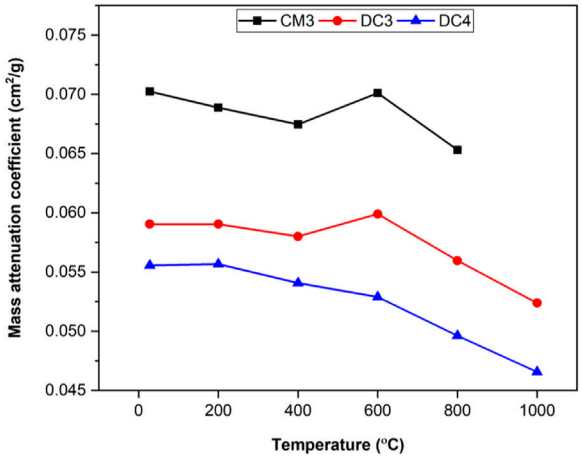

FIGURE 17
Mass Attenuation Coefficient as function of temperature.

attenuation is measured for DC3 concrete, whereas the highest was measured for DC4 concrete. Linear attenuation depends upon the density of the material. Since DC4 concrete exhibit more density among all mixes, therefore, linear attenuation was measured highest for this mix. It may also be noted that a sharp decrease in attenuation properties for all mixes was noted at 600°C since the compressive strength drastically decreased in mixes due to chemical and physical changes that occurred at this stage of heating. As shown in the figure, the control mix (CM1) decreases from room temperature to 400°C and then increases to 600°C. This is because gamma ray exhibits a shorter wavelength, less than 100 pm. It may be possible that the gamma-ray strike with heavy aggregate or cement particles at this temperature range tends to attenuate more compared to mixes at different temperatures (Khan et al., 2022). The attenuation of CM1 mix at 1000°C could not be measured due to complete disintegration and decomposition.

3.7.2 Mass attenuation coefficient (MAC)

Mass attenuation is the function of linear attenuation with respect to density of the material. The mass attenuation of CM3, DC3 and DC4 at various temperatures is shown in Figure 17. Since the DC4 exhibit the highest density among all the mixes, the mass attenuation was measured maximum for this mix. Additionally, DC4 concrete attenuation increased at 200°C, which may be evident of reverse hydration of un-hydrated cement. These values then tend to decrease at all temperatures. The DC3 mix showed more attenuation at room temperature than the CM3 mix. However, this value decreased at all temperatures later. There may be a few reasons that could explain this phenomenon such as bad mix where

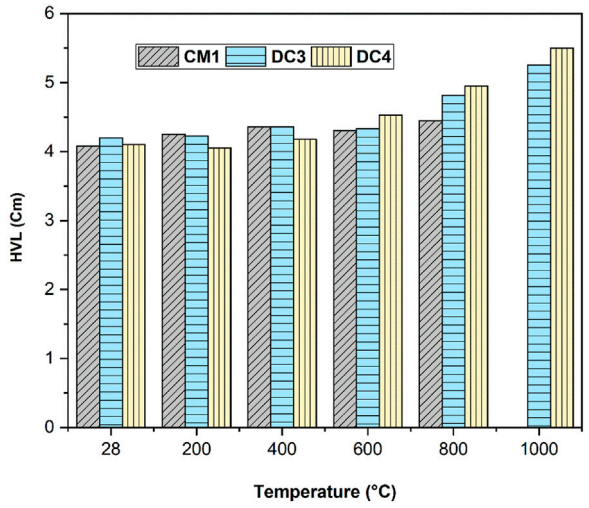

FIGURE 18
Half Value Layer (HVL) as function of temperature.

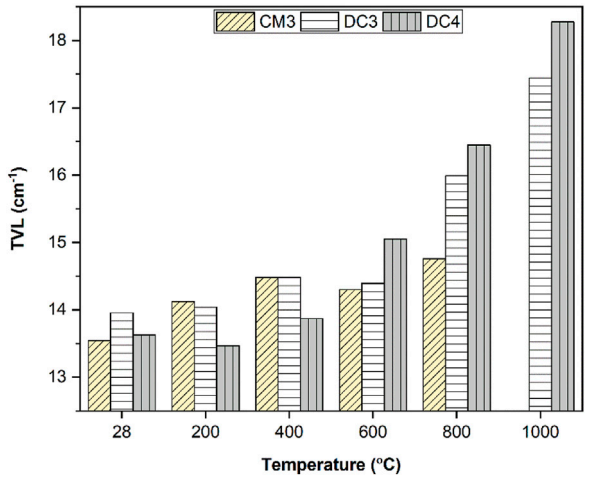

FIGURE 19
Tenth Value Layer (TVL) as a function of temperature.

the aggregates were clustered at once and not mixed thoroughly or due to the bad geometry of the gamma-ray setup (Lee et al., 2007; Kumar et al., 2021; Ouda, 2021).

3.7.3 Half Value Layer (HVL) and 10th Value Layer (TVL)

The HVL and TVL values of the control mix and dolerite mixes are shown in Figure 18 and Figure 19, respectively.

Both attenuation properties tend to rise by increasing the temperature. For instance, the HVL value of DC3 mix was found to be 4.1 Cm at ambient temperature where it was noted 4.8 cm at 800°C. Figure 18 also show that dolerite mixes (DC3 and DC4) exhibit lowest HVL values compared to control mix up to 600°C. However, beyond this temperature, the HVL values tends to increase by increasing temperature.

The same trend could be noted in TVL values. At ambient temperature, the TVL was found to be maximum for DC4 concrete and minimum for DC3 concrete. This trend was followed until the temperature reached 600°C, where the TVL increased linearly for DC4 mixes. The phenomena of increase and decrease have already been explained in sections 4.3, 4.4, and 4.6.1.

4 Conclusion

This paper investigates the physical, mechanical, and microstructural properties as well as X-ray and gamma rays attenuation measured for heavy-density dolerite concrete at temperatures of 200°C–1200°C. The study provides comprehensive experimental results which will be helpful in assessing the various properties of concrete as gamma ray shield at high temperatures. The following concluding remarks are drawn.

1) At all temperatures, the mass, and density loss were more pronounced in control mixes compared to dolerite mixes. The lowest density loss was observed for mixes with 75% dolerite aggregate.
2) Specimens with 75% dolerite aggregate mix showed a compressive strength of 57.6 MPa, more than the control mix1, control mix2, and control mix 3 by 31.9%, 29.3%, and 24.8%, respectively, at room temperature. The concrete with 75% dolerite aggregates showed a loss in compressive strength of 4.50%, 8.50%, 27.0%, 55.0%, 80.0%, and 65.0% at 200°C, 400°C, 600°C, 800°C, and 1000°C, respectively compared to room temperature.
3) The rebound hammer followed the same pattern of compressive strength for control and dolerite mixes at all temperatures. The X-ray radiography showed gas pores, bond, and matrix cracks as well as voids in post-heated specimens whereas showed a compact structure in pre-heated specimens.
4) Linear attenuation coefficient (LAC) values were found more for control mixes whereas less for mix incorporated with 100% dolerite aggregate. The linear attenuation coefficient is a function of thickness thus increasing the thickness tends to increase LAC.
5) Mass attenuation coefficient (MAC) is a function of the density of material therefore the specimen with 100% dolerite aggregates exhibited the lowest MAC because of the higher density among other mixes. The Half Value Layer (HVL) and Tenth Value Layer (TVL) followed the pattern of LAC and MAC at all temperatures. The specimen with 100% dolerite aggregates showed the highest attenuation of gamma rays to one-fifth and one-tenth levels.

Data availability statement

The original contributions presented in the study are included in the article/supplementary material, further inquiries can be directed to the corresponding author.

Author contributions

The author and contributions to the paper are as follows: MK and MY proposed the idea and designed the experimental program; AM

reviewed and formulated a design for gamma radiation, MU, MAb, and HA conducted the tests and analyzed the data; MN helped in arranging test data and writing the paper, AM and SA reviewed the paper. All authors contributed to the writing of the paper.

Acknowledgments

The authors are extremely grateful to Engr. Mir Qad MA (Head, foundry section, HMC, Taxila, Pakistan) for providing free heating and X-ray services. In addition, the authors would like to thank Noor Nawaz Khan for supplying free of cost dolerite aggregates from mines in Mansehra, Pakistan. The authors thank the NERML, PIEAS staff for their assistance in measuring the attenuation of concrete.

Conflict of interest

The authors declare that the research was conducted in the absence of any commercial or financial relationships that could be construed as a potential conflict of interest.

Publisher's note

References

Akkurt, I., and El-Khayatt, A. M. (2013). The effect of barite proportion on neutron and gamma-ray shielding. *Ann. Nucl. Energy* 51, 5–9. doi:10.1016/j.anucene.2012.08.026

Almeida, J., Airton, T., Nogueira, M. S., Vivolo, V., Potiens, M. P. A., and Campos, L. L. (2017). Mass attenuation coefficients of X-rays in different barite concrete used in radiation protection as shielding against ionizing radiation. *Radiat. Phys. Chem.* 140, 349–354. doi:10.1016/j.radphyschem.2017.02.054

AMERICAN SOCIETY FOR TESTING AND MATERIALS (ASTM) (2015). *'Astm C39'. Standard test method for compressive strength of cylindrical concrete Specimens1 i*, 1–7. doi:10.1520/C0039

Behnood, A. (2014). *High-strength concrete incorporating copper slag and ground pumice*. Sydney: Master Thesis March.

Burrow, R C., Griswold, G D., and Barry Oland, C. (1979). Properties of concrete at elevated temperatures. *Desalination*, 429–432.

Celik, K., Meral, C., Gursel, A. P., Kumar Mehta, P., Horvath, A., Paulo, J., et al. (2015). Mechanical properties, durability, and life-cycle assessment of self-consolidating concrete mixtures made with blended Portland cements containing fly ash and limestone powder. *Cem. Concr. Compos.* 56, 59–72. doi:10.1016/j.cemconcomp.2014.11.003

Chang, W T., ChenWang, T., Huang, C W., and Giang, Y-S. (1994). Concrete at temperatures above 1000°C. *Fire Saf. J.* 23 (3), 223–243. doi:10.1016/0379-7112(94)90030-2

Diamond, S., and Huang, J. (2001). The itz in concrete - a different view based on image analysis and SEM observations. *Cem. Concr. Compos.* 23 (2–3), 179–188. doi:10.1016/S0958-9465(00)00065-2

El-Samrah, G. M., Moamen, G., Abdel-Rahman, M A. E., and el Shazly, R. M. (2018). Effect of heating on physical, mechanical, and nuclear radiation shielding properties of modified concrete mixes. *Radiat. Phys. Chem.* 153, 104–110. doi:10.1016/j.radphyschem.2018.09.018

Facure, A., and Silva, A. X. (2007). The use of high-density concretes in radiotherapy treatment room design. *Appl. Radiat. Isotopes* 65 (9), 1023–1028. doi:10.1016/j.apradiso.2007.04.006

Fillmore, D. L. (2004). *Literature review of the effects of radiation and temperature on the aging of concrete*. Idaho: Idaho National Engineering and Environmental Laboratory. September: 1–26.

Gencel, O., Koksal, F., Ozel, C., and Brostow, W. (2012). Combined effects of fly ash and waste ferrochromium on properties of concrete. *Constr. Build. Mater.* 29, 633–640. doi:10.1016/j.conbuildmat.2011.11.026

Gökçe, H. S., Öztürk, B. C., Çam, N. F., and Andiç-Çakır, Ö. (2018). Gamma-ray attenuation coefficients and transmission thickness of high consistency heavyweight concrete containing mineral admixture. *Cem. Concr. Compos.* 92, 56–69. doi:10.1016/j.cemconcomp.2018.05.015

González-Ortega, M. A., Segura, I., Cavalaro, S. H. P., Toralles-Carbonari, B., Aguado, A., and Andrello, A. C. (2014). Radiological protection and mechanical properties of concretes with EAF steel slags. *Constr. Build. Mater.* 51, 432–438. doi:10.1016/j.conbuildmat.2013.10.067

Hager, I. (2013). Behaviour of cement concrete at high temperature. *Bull. Pol. Acad. Sci. Tech. Sci.* 61 (1), 145–154. doi:10.2478/bpasts-2013-0013

Hernandez-Murillo, G., Geovanni, C., Rafael Molina Contreras, J., Escalera-Velasco, L A., Leon-Martínez, H A d., Rodriguez-Rodriguez, J A., et al. (2020). X-ray and gamma ray shielding behavior of concrete blocks. *Nucl. Eng. Technol.* 52 (8), 1792–1797. doi:10.1016/j.net.2020.01.007

Horszczaruk, E., and Brzozowski, P. (2019). Investigation of gamma ray shielding efficiency and physicomechanical performances of heavyweight concrete subjected to high temperature. *Constr. Build. Mater.* 195, 574–582. doi:10.1016/j.conbuildmat.2018.09.113

Horszczaruk, E. (2019). Properties of cement-based composites modified with magnetite nanoparticles: A review. *Materials* 12 (2), 326. doi:10.3390/ma12020326

Ingham, J P. (2013). Building stone. *Geomaterials Under Microsc.* 21, 21–50. doi:10.1016/b978-0-12-407230-5.50010-8

Kansouh, W. A. (2012). Radiation distribution through serpentine concrete using local materials and its application as a reactor biological shield. *Ann. Nucl. Energy* 47, 258–263. doi:10.1016/j.anucene.2012.05.008

Khan, M. N. A., Yaqub, M., and Malik, Azhar H. (2022). High density concrete incorporating grit scale aggregates for 4th generation nuclear power plants. *Constr. Build. Mater.* 337, 127578. doi:10.1016/j.conbuildmat.2022.127578

Khalaf, M A., Ban, C. C., and Ramli, M. (2019). The constituents, properties and application of heavyweight concrete: A review. *Constr. Build. Mater.* 215, 73–89. doi:10.1016/j.conbuildmat.2019.04.146

Khalaf, M A., Cheah, C B., Ramli, M., Ahmed, N M., and Al-Shwaiter, A. (2021). Effect of nano zinc oxide and silica on mechanical, fluid transport and radiation attenuation properties of steel furnace slag heavyweight concrete. *Constr. Build. Mater.* 274, 121785. doi:10.1016/j.conbuildmat.2020.121785

Kilincarslan, S., Akkurt, I., and Basyigit, C. (2006). The effect of barite rate on some physical and mechanical properties of concrete. *Mater. Sci. Eng. A* 424 (1–2), 83–86. doi:10.1016/j.msea.2006.02.033

Koťátková, J., Jan, Z., Reiterman, P., Jan, P., Hlaváč, Z., and Brabec, P. (2016). The effect of elevated temperatures and nuclear radiation on the properties of biological shielding concrete. *Key Eng. Mater.* 677, 8–16. doi:10.4028/www.scientific.net/kem.677.8

Kumar, S., Mann, K S., Singh, T., and Singh, S. (2021). Investigations on the gamma-ray shielding performance of green concrete using theoretical, experimental and simulation techniques. *Prog. Nucl. Energy* 134, 103654. doi:10.1016/j.pnucene.2021.103654

Lamarsh, J R., Baratta, A J. B. n. d., Lamarsh, A. J., and John, R. (2014). *Introduction to nuclear engineering-pearson* `. Edinburgh: Pdf.

Lee, C-m, YoonLee, H, and Lee, K J (2007). Cracking effect on gamma-ray shielding performance in concrete structure. *Prog. Nucl. Energy* 49, 303–312. doi:10.1016/j.pnucene.2007.01.006

Lotfi-omran, O., Ali, S., and ImanNikbin, M. (2019). A comprehensive study on the effect of water to cement ratio on the mechanical and radiation shielding properties of heavyweight concrete. *Constr. Build. Mater.* 229, 116905. doi:10.1016/j.conbuildmat.2019.116905

Malik, A H., Ayaz, N., Khan, M., Yaqub, M., and Gul, A. (2022). *Recent developments in concrete as a gamma ray shielding material*. doi:10.31031/ACET.2022.05.000609

Maslehuddin, M., Naqvi, A. A., Ibrahim, M., and Kalakada, Z. (2013). Radiation shielding properties of concrete with electric arc furnace slag aggregates and steel shots. *Ann. Nucl. Energy* 53, 192–196. doi:10.1016/j.anucene.2012.09.006

Mehdipour, S., Nikbin, I M., Dezhampanah, S., Mohebbi, R., Moghadam, H H., Charkhtab, S., et al. (2020). Mechanical properties, durability and environmental evaluation of rubberized concrete incorporating steel fiber and metakaolin at elevated temperatures. *J. Clean. Prod.* 254, 120126. doi:10.1016/j.jclepro.2020.120126

Method, Standard Test (1998). *'Standard test method for rebound number of hardened concrete 1'*. Concrete *14*. nurol llc), 1–3. Available at:.

Mohammed Haneefa, K., Santhanam, Manu, and Parida, F. C. (2013). Review of concrete performance at elevated temperature and Hot sodium exposure applications in nuclear industry. *Nucl. Eng. Des.* 258, 76–88. doi:10.1016/j.nucengdes.2013.01.018

Moharram, B. M., Nagy, M. E., Shaat, M K., el Sayed, A. R., Fayiz, M., Dwidar, Samy A., et al. (2020). Performance of lead and iron oxides nanoparticle materials on shielding properties for γ-rays. *Radiat. Phys. Chem.* 173, 108880. doi:10.1016/j.radphyschem.2020.108880

Mollah, A. S., Ahmad, G. U., and Husain, S. R. (1992). Measurements of neutron shielding properties of heavy concretes using a Cf-252 source. *Nucl. Eng. Des.* 135 (3), 321–325. doi:10.1016/0029-5493(92)90199-6

Monte, F lo, and Pietro, G. G. (2014). Thermo-mechanical behavior of baritic concrete exposed to high temperature. *Cem. Concr. Compos.* 53, 305–315. doi:10.1016/j.cemconcomp.2014.07.009

Naus, D. 2010. 'A compilation of elevated temperature concrete material property data and information for use in assessments of nuclear power plant reinforced concrete structures', 328.

Nikbin, I M., Mehdipour, S., Dezhampanah, S., Mohammadi, R., Mohebbi, R., Moghadam, H., et al. (2020). Sadegh mehdipour, soudabeh dezhampanah, reza mohammadi, reza mohebbi, Hamid Habibi moghadam, and ali SadrmomtaziEffect of high temperature on mechanical and gamma ray shielding properties of concrete containing nano-TiO2. *Radiat. Phys. Chem.* 174, 108967. doi:10.1016/j.radphyschem.2020.108967

Ouda, A. S. (2021). A preliminary investigation on gamma-rayattenuation of alkali-activated concrete waste based-geopolymer modified with pozzocrete-fly ash. *Prog. Nucl. Energy* 134, 103681. doi:10.1016/j.pnucene.2021.103681

Ouda, A S. (2015). Development of high-performance heavy density concrete using different aggregates for gamma-ray shielding. *HBRC J.* 11 (3), 328–338. doi:10.1016/j.hbrcj.2014.06.010

Ouda, A S., and Abdel-Gawwad, H A. (2017). The effect of replacing sand by iron slag on physical, mechanical and radiological properties of cement mortar. *HBRC J.* 13 (3), 255–261. doi:10.1016/j.hbrcj.2015.06.005

Powe, A., Szulej, J., and Ogrodnik, P. (2020). Effect of high temperatures on the impact strength of concrete based on recycled aggregate made of Heat-resistant cullet. *Materials* 13 (2), 465–486. doi:10.3390/ma13020465

Sadrmomtazi, A., Sobhani, J., Mirgozar, M. A., and Najimi, M. (2012). Properties of multi-strength grade EPS concrete containing silica fume and rice Husk ash. *Constr. Build. Mater.* 35, 211–219. doi:10.1016/j.conbuildmat.2012.02.049

Sakr, K., and El-Hakim, E. (2005). Effect of high temperature or fire on heavy weight concrete properties. *Cem. Concr. Res.* 35 (3), 590–596. doi:10.1016/j.cemconres.2004.05.023

Shirayama, K. (1963). Properties of radiation shielding concrete'. *ACI J. Proc.* 60 (2). doi:10.14359/7855

Shumuye, E D., Zhao, J., and Wang, Z. (2019). Effect of fire exposure on physico-mechanical and microstructural properties of concrete containing high volume slag cement. *Constr. Build. Mater.* 213, 447–458. doi:10.1016/j.conbuildmat.2019.04.079

Sikora, P., Abd Elrahman, M., Horszczaruk, E., Brzozowski, P., and Stephan, D. (2019). Incorporation of magnetite powder as a cement additive for improving thermal resistance and gamma-ray shielding properties of cement-based composites. *Constr. Build. Mater.* 204, 113–121. doi:10.1016/j.conbuildmat.2019.01.161

Singh, S.l, and Singh, K. (2021). On the use of green concrete composite as a nuclear radiation shielding material. *Prog. Nucl. Energy* 136, 103730. doi:10.1016/j.pnucene.2021.103730

Sivathanu Pillai, C., Santhakumar, A. R., Poonguzhali, A., Pujar, M. G., Ashok Kumar, J., Preetha, R., et al. (2016). Evaluation of microstructural and microchemical aspects of high density concrete exposed to sustained elevated temperature. *Constr. Build. Mater.* 126, 453–465. doi:10.1016/j.conbuildmat.2016.09.053

Sloane, D. J. (1991). Some physical properties of dolerite. *Cercet. Agron. În Mold.* XLIII (1), 17–29. Available at:.

Tekin, H. O., Sayyed, M. I., and Issa, S A. M. (2018). Gamma radiation shielding properties of the Hematite-serpentine concrete blended with WO3 and Bi2O3 micro and nano particles using MCNPX code. *Radiat. Phys. Chem.* 150, 95–100. doi:10.1016/j.radphyschem.2018.05.002

Thomas, C., Rico, J., Tamayo, P., Ballester, F., Setién, J., and Polanco, J. A. (2019). Effect of elevated temperature on the mechanical properties and microstructure of heavy-weight magnetite concrete with steel fibers. *Cem. Concr. Compos.* 103, 80–88. doi:10.1016/j.cemconcomp.2019.04.029

Topçu, I B. (2003). Properties of heavyweight concrete produced with barite. *Cem. Concr. Res.* 33 (6), 815–822. doi:10.1016/S0008-8846(02)01063-3

Yao, Y., Zhang, X., Li, M., Yang, R., Jiang, T., and Lv, J. (2016). Investigation of gamma ray shielding efficiency and mechanical performances of concrete shields containing bismuth oxide as an environmentally friendly additive. *Radiat. Phys. Chem.* 127, 188–193. doi:10.1016/j.radphyschem.2016.06.028